Cantu syndrome–associated SUR2 (ABCC9) mutations in distinct structural domains result in K_{ATP} channel gain-of-function by differential mechanisms

Received for publication, October 9, 2017, and in revised form, December 20, 2017 Published, Papers in Press, December 22, 2017, DOI 10.1074/jbc.RA117.000351

Conor McClenaghan[‡], Alex Hanson[‡], Monica Sala-Rabanal[‡], Helen I. Roessler[§1], Dragana Josifova[¶], Dorothy K. Grange[‖], Gijs van Haaften[§], and Colin G. Nichols[‡2]

From the Departments of [‡]Cell Biology and Physiology and [‖]Pediatrics, Center for the Investigation of Membrane Excitability Diseases, Washington University School of Medicine, Saint Louis, Missouri 63110, the [§]Department of Medical Genetics, University Medical Center Utrecht, Postbus 85500, 3508 GA Utrecht, The Netherlands, and the [¶]Guy's and St. Thomas NHS Trust, Clinical Genetics Department, Great Maze Pond, London SE1 9RT, United Kingdom

Edited by Henrik G. Dohlman

The complex disorder Cantu syndrome (CS) arises from gain-of-function mutations in either *KCNJ8* or *ABCC9*, the genes encoding the Kir6.1 and SUR2 subunits of ATP-sensitive potassium (K_{ATP}) channels, respectively. Recent reports indicate that such mutations can increase channel activity by multiple molecular mechanisms. In this study, we determined the mechanism by which K_{ATP} function is altered by several substitutions in distinct structural domains of SUR2: D207E in the intracellular L0-linker and Y985S, G989E, M1060I, and R1154Q/R1154W in TMD2. We engineered substitutions at their equivalent positions in rat SUR2A (D207E, Y981S, G985E, M1056I, and R1150Q/R1150W) and investigated functional consequences using macroscopic rubidium ($^{86}Rb^+$) efflux assays and patch-clamp electrophysiology. Our results indicate that D207E increases K_{ATP} channel activity by increasing intrinsic stability of the open state, whereas the cluster of Y981S/G985E/M1056I substitutions, as well as R1150Q/R1150W, augmented Mg-nucleotide activation. We also tested the responses of these channel variants to inhibition by the sulfonylurea drug glibenclamide, a potential pharmacotherapy for CS. None of the D207E, Y981S, G985E, or M1056I substitutions had a significant effect on glibenclamide sensitivity. However, Gln and Trp substitution at Arg-1150 significantly decreased glibenclamide potency. In summary, these results provide additional confirmation that mutations in CS–associated SUR2 mutations result in K_{ATP} gain-of-function. They help link CS genotypes to phenotypes and shed light on the underlying molecular mechanisms, including consequences for inhibitory drug sensitivity, insights that may inform the development of therapeutic approaches to manage CS.

ATP-sensitive potassium (K_{ATP}) channels are potassium-selective ion channels formed by obligate co-assembly of pore-forming Kir6.x subunits and regulatory sulfonylurea receptors (SURx)[3] in a 4:4 stoichiometry (1–4). Channel opening is dynamically regulated by intracellular nucleotides and membrane phospholipids and thereby couples the membrane potential of excitable cells to their metabolic state (5). By binding to, and stabilizing, closed states of the Kir6.x subunit, ATP decreases channel open probability, whereas magnesium-nucleotide complexes (MgADP and MgATP) bind to the nucleotide-binding domains (NBDs) of SURx subunits to activate the channel (6, 7).

In cardiac, smooth, and skeletal muscle, SUR2 subunits (of which there are two main splice variants, SUR2A and SUR2B) co-assemble variously with Kir6.1 (as in vascular smooth muscle) or Kir6.2 (as in ventricular and skeletal muscle) (8, 9). In the heart, Kir6.2/SUR2A K_{ATP} channels have been proposed to be critical for ischemic pre-conditioning, whereas in skeletal muscle Kir6.2/SUR2A channels may provide a "brake" to hyperpolarize the membrane potential despite elevations in intracellular calcium during periods of exercise and increased metabolism (9, 10). In smooth muscle, Kir6.1/SUR2B K_{ATP} activity is a key determinant of electrical excitability and consequent contractility in blood and lymphatic vessels, as well as in bladder and uterine muscle (11–15).

There have now been multiple reports of mutations in the *ABCC9* and *KCNJ8* genes (which encode SUR2 and Kir6.1, respectively) associated with the complex heritable disorder, Cantu syndrome (CS) (16–21). CS patients exhibit diverse cardiovascular features, including dilated and tortuous vessels, cardiomegaly, electrophysiological alterations in the cardiac conduction system, decreased neurovascular coupling, and persistence of fetal circulation (16–18, 20–25). An emerging model for the molecular basis of CS is that missense mutations in *ABCC9* or *KCNJ8* result in increased K_{ATP} channel activity and consequently reduced smooth muscle excitability and contractility (26, 27). CS–associated mutations in SUR2 have previously been shown to result in K_{ATP} channel gain-of-function (GoF) by distinct mechanisms, including enhanced Mg^{2+}-nu-

This work was supported in part by National Institutes of Health Grant HL140024 from NHLBI (to C. G. N.). The authors declare that they have no conflicts of interest with the contents of this article. The content is solely the responsibility of the authors and does not necessarily represent the official views of the National Institutes of Health.

[1] Supported by the E-Rare Joint Transnational Cantu Treat Program Grant I-2101-B26 (to G. v. H.).

[2] To whom correspondence should be addressed. Tel.: 314-362-6630; Fax: 314-362-7463; E-mail: cnichols@wustl.edu.

[3] The abbreviations used are: SU, sulfonylurea; SUR, sulfonylurea receptor; CS, Cantu syndrome; NBD, nucleotide-binding domain; DMEM, Dulbecco's modified Eagle's medium; GoF, gain-of-function; MI, metabolic inhibition; PIP_2, L-α-phosphatidylinositol-4,5-bisphosphate; TM, transmembrane.

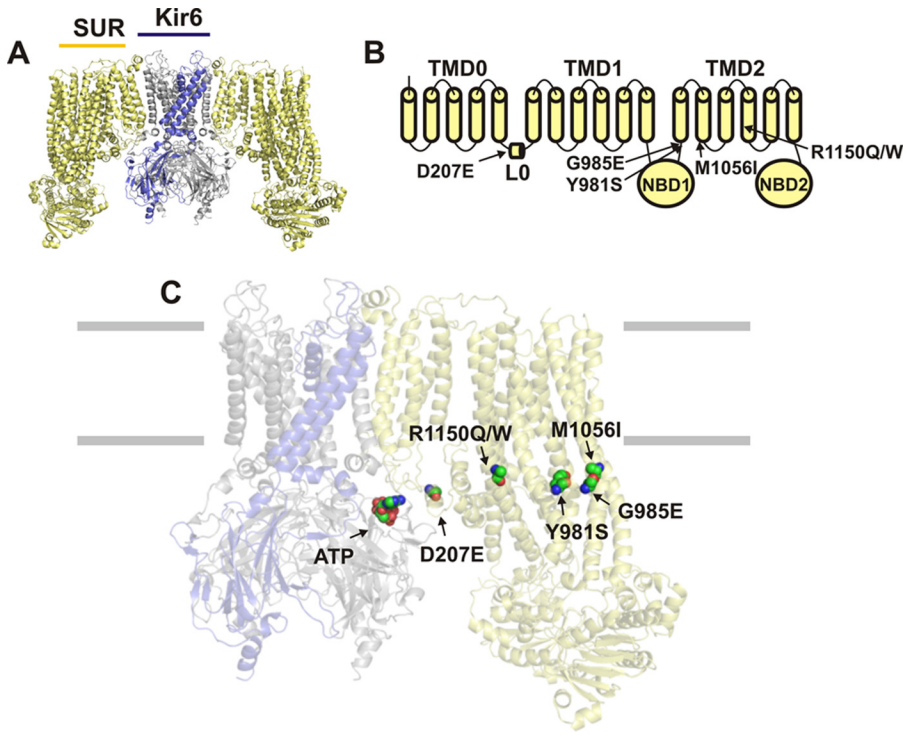

Figure 1. Structure of K_{ATP} channels. *A*, K_{ATP} channels form as hetero-octamers of four pore-forming Kir6.x subunits each associated with a SUR subunit (two SUR subunits omitted from figure). *B*, schematic representation of the position of D207E, Y981S, G985E, M1056I, and R1150Q/R1150W in the linear sequence of SUR2. *C*, expected positions of D207E, Y981S, G985E, M1056I, and R1150Q/R1150W mapped onto the pancreatic K_{ATP} (Kir6.2/SUR1; Protein Data Bank code 5WUA) structure (4). The residues shown are the analogous positions in hamster SUR1 (Asp-209, Tyr-1004, Ala-1008, Thr-1089, and Arg-1183, respectively; there is 70% sequence identity between hSUR1 and rSUR2A, and structural the domains are expected to be conserved). ATP is modeled in the Kir6.2-binding site.

cleotide activation and increased intrinsic open probability with consequent decreases in ATP inhibition (18, 19). Here, we examined the functional effects of previously uncharacterized CS mutations that are predicted to cluster together at the link between NBD1 and TMD2: Y981S (human Y985S), G985E (G989E), and M1056I (M1060I) (Fig. 1), and we compared the molecular consequences to those of D207E, located in the intracellular L0-linker, between TMD0 and TMD1 (Fig. 1). In addition, the sensitivity of mutant channels to the sulfonylurea K_{ATP}-inhibitor glibenclamide was tested. Glibenclamide holds promise as a potential treatment for CS, although numerous Kir6.2- and SUR1-dependent K_{ATP} GoF mutations, which reduce sulfonylurea sensitivity, have previously been reported (28–30). Therefore, determining sulfonylurea sensitivity for specific mutations may be required for future individualized therapy. The results are interpreted alongside structural insights from recently reported high resolution cryo-EM structures of K_{ATP} channel complexes (3, 4) to provide further detail of the molecular basis of K_{ATP} channel GoF in CS.

Results

Case history of subject with SUR2(Y985S) mutation

The subject is the fourth child of healthy, unrelated Caucasian parents, with no family history of relevance to her condition. The pregnancy was complicated with raised nuchal translucency at 12 weeks and polyhydramnios at 32 weeks of gestation. At 38 weeks of gestation, labor was induced, with uncomplicated vaginal delivery. Birth weight was 5.3 kg (>99 centile). There was no significant delay in early development, but language skills developed slowly. At birth, hypertrichosis was evident, with a full head of dark hair with low anterior hairline; shoulders, arms, legs, and back were covered with long, thick, and dark hair. At 3 years of age, facial features were rather coarse, with mild epicanthic folds and down-slanting palpable fissures with full lips and a broad face. The forehead was extremely low with fine hair in front of the ears, extending over her chin, and hypertrichosis over her neck and chest. The heart was slightly enlarged, but there was no overt evidence of cardiomyopathy.

At age 5, the subject presented with recurrent respiratory infections and required hospital admission for pneumonia, leading to tonsillectomy and adenoidectomy, which improved severe snoring and obstructive sleep apnea. Height was on the 50th centile, weight on the 91st centile, and her head circumference was on the 98th centile. Facial features remained coarse with down-slanting palpable fissures, full cheeks, broad tip to the nose with mild thickening of the alae nasae, and a low columella. Significant joint laxity was evident in the hands, with deep palmar creases and soft skin on the palms and generous fetal finger pads.

This subject thus exhibited most of the features typically found in individuals with CS (18, 24). Sequencing of *ABCC9*-coding regions revealed a heterozygous mutation (c.2954A→C, p.Y985S) that was absent in genomic DNA from either parent. Heterozygous *de novo* mutations (p.G989E; p.M1060I) were also identified in two additional diagnosed CS subjects, for whom clinical details are not available. The three mutated residues are predicted to cluster in a similar location within the SUR2 protein (Fig. 1). We therefore analyzed the molecular consequences of these mutations and compared them with the

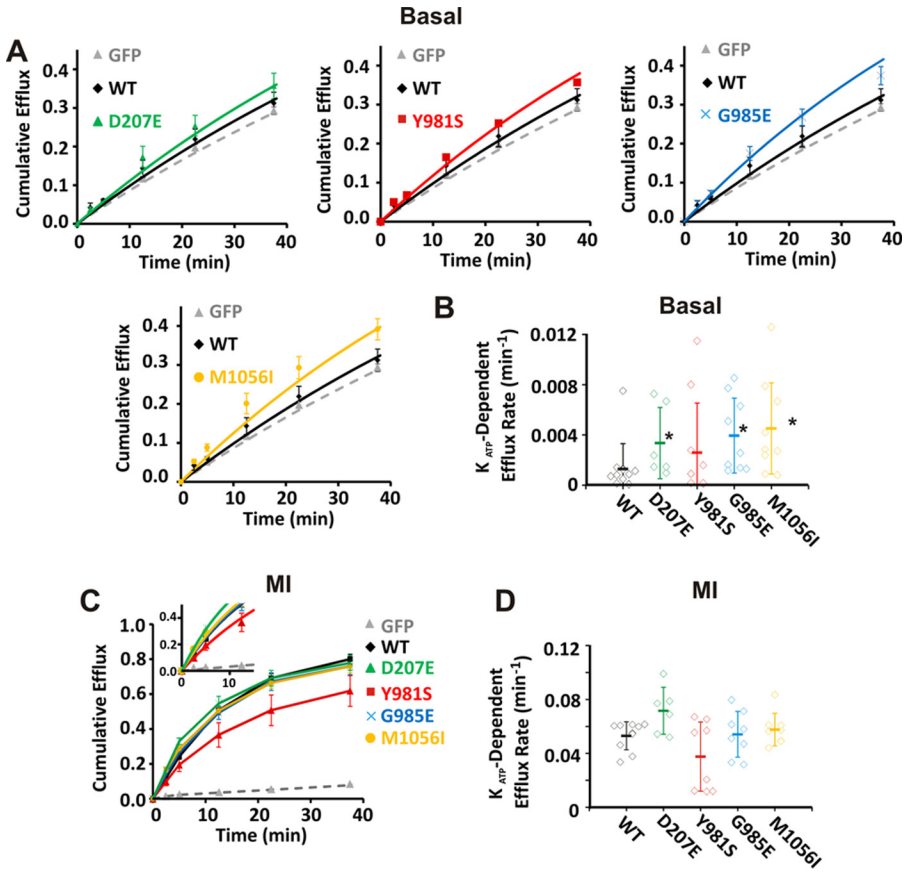

Figure 2. D207E, G985E, and M1056I significantly increase basal K_{ATP} channel activity in intact cells. *A*, cumulative $^{86}Rb^+$ efflux was measured from Cosm6 cells transfected either with GFP alone or with Kir6.2 plus WT or mutant SUR2A. Efflux as a function of time was first recorded in basal conditions (cells incubated in Ringer's solution) (*A*), and the K_{ATP}-dependent efflux rate was attained from exponential fits to efflux time data (*B*). Second, efflux was measured from cells subjected to MI (induced by incubation in Ringer's solution with 2.5 mg/ml oligomycin and 1 mM 2-deoxy-D-glucose from 10 min prior to commencing the flux assay) (*C*), and the rate constant for K_{ATP}-dependent efflux in MI was calculated from exponential fits to the early time points (2.5, 5, and 12.5 min) (*inset, C* and *D*). Efflux-time data are shown as mean ± S.E., and K_{ATP}-dependent efflux rate scatter plots show mean ± S.D. from 3 to 5 independent experiments. Statistical significance is denoted by *asterisk* and defined as $p < 0.05$ according to Mann-Whitney *U* test.

consequences of the most common CS mutation (p.R1154Q), and another uncharacterized CS mutation p.D207E (16), located in distinct SUR2 domains.

Cantu syndrome mutations result in gain-of-function of K_{ATP} channel in intact cells

To determine the effect of mutations on K_{ATP} channel function, SUR2A constructs were co-expressed with Kir6.2 in Cosm6 cells, and channel activity was assessed using a radioactive $^{86}Rb^+$ flux assay. First, basal K_{ATP} activity under quasi-physiological regulation by intracellular nucleotides in intact cells was determined by measuring $^{86}Rb^+$ efflux from cells bathed in Ringer's solution. As shown in Fig. 2, *A* and *B*, the K_{ATP}-dependent $^{86}Rb^+$ efflux rate in these conditions was significantly increased by the D207E, G985E, and M1056I substitutions, although a trend toward an increase was observed for Y981S. Efflux rates in basal conditions are a function of both channel activity and surface membrane expression. We assessed efflux rates in cells subjected to metabolic inhibition (MI) to decrease intracellular ATP synthesis and relieve channels of nucleotide regulation. Assuming that the single channel conductance is unaffected and that MI maximally activates available channels, the comparison of the MI efflux rate between constructs provides an estimation of the relative number of channels in the membrane. As shown in Fig. 2, *C* and *D*, there was a statistically insignificant decrease in Y981S efflux rate, and a statistically insignificant increase in MI efflux rate was observed for D207E, implying that these mutations result in only a small decrease or increase, respectively, in channel number. Otherwise, the maximum flux under these conditions was not markedly different between constructs, suggesting that the number of active channels was similar.

All known CS patients are heterozygous, and we modeled heterozygous conditions by co-expressing Kir6.2 together with WT SUR2A and mutant SUR2A subunits at a 1:1 ratio. The resultant channels were assayed by monitoring $^{86}Rb^+$ efflux. Only very minor increases in basal efflux rate were observed for D207E, G985E, and M1056I, although a moderate, statistically significant increase was observed for Y981S channels (Fig. 3). Taken together, these data demonstrate that whereas all tested mutations result in K_{ATP} gain-of-function, in heterozygous conditions the effect is subtle under basal conditions.

D207E in the L0-linker increases open-state stability and decreases ATP inhibition

Increased basal K_{ATP} channel activity could arise from changes in multiple distinct nucleotide-sensing mechanisms,

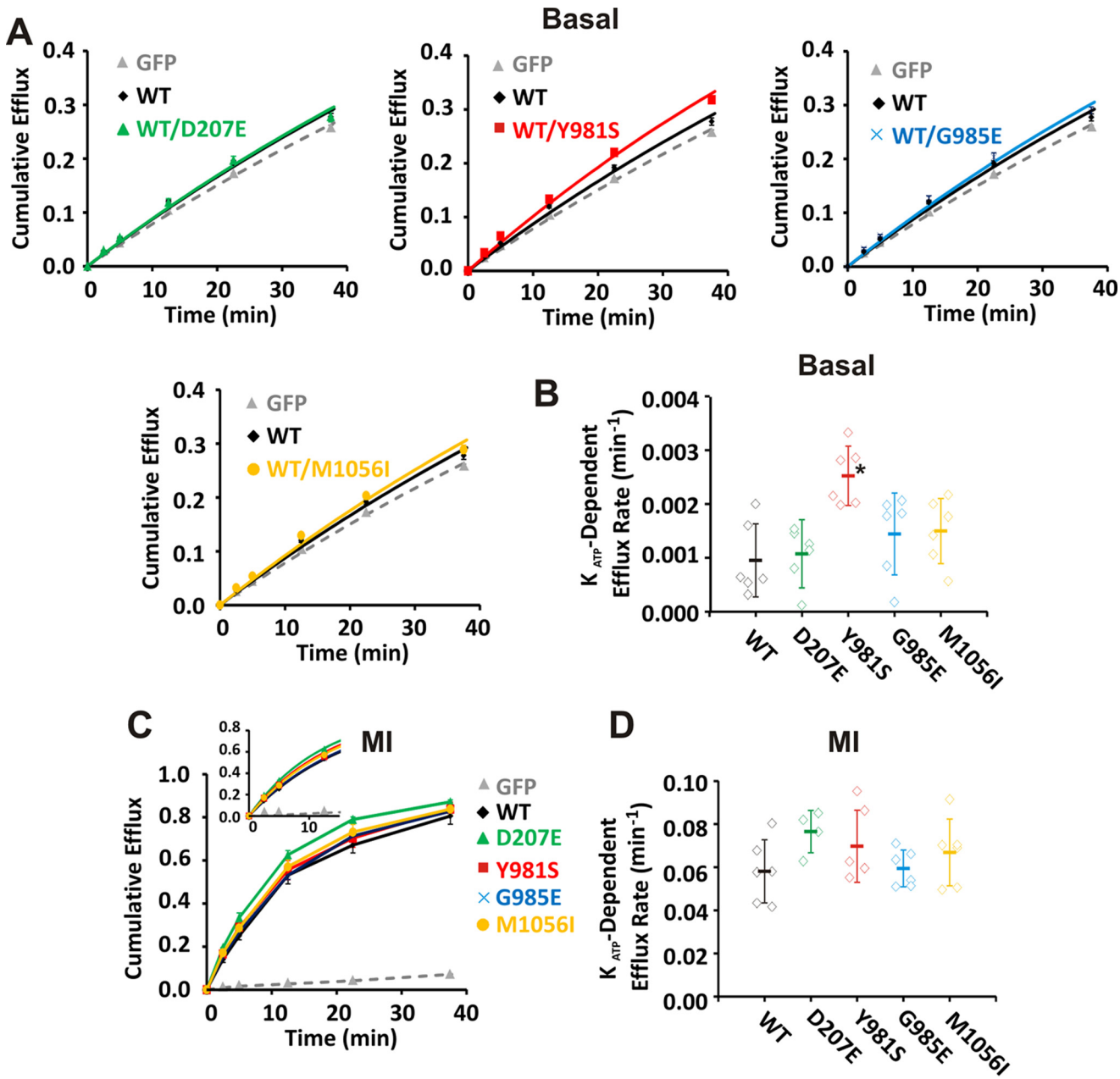

Figure 3. Y981S confers gain-of-function when co-expressed with WT subunits in intact cells whereas only minor effects are observed for other mutations. Cumulative $^{86}Rb^+$ efflux was measured from Cosm6 cells transfected either with GFP alone or with Kir6.2 alongside SUR2A-WT alone or SUR2A-WT with mutant SUR2A at a 1:1 ratio. Basal efflux shown as function of time (*A*), and K_{ATP}-dependent efflux rate constants were calculated (*B*). Efflux rate was measured in MI conditions (induced by incubation in Ringer's solution with 2.5 mg/ml oligomycin and 1 mM 2-deoxy-D-glucose from 10 min prior to commencing the flux assay) (*C*), and rate constants were calculated from early time points (2.5, 5, and 12.5 min) (*inset, C* and *D*). Efflux-time data are shown as mean ± S.E., and K_{ATP}-dependent efflux rate scatter plots show mean ± S.D. from 3 to 5 independent experiments. Statistical significance is denoted by *asterisk* and defined as $p < 0.05$ according to Mann-Whitney *U* test.

including increased Mg-nucleotide activation or decreased ATP inhibition, either as a result of decreased binding affinity or decreased efficacy due to increase in intrinsic open-state stability (19). To investigate the effects of the above mutations on nucleotide sensitivity, we used inside-out patch-clamp recordings. As shown in Fig. 4, channels comprising Kir6.2 and WT SUR2A were inhibited by ATP in the absence of Mg^{2+} with an IC_{50} of ~15 μM. In the presence of Mg^{2+}, the IC_{50} was ~20 μM. The presence of Mg^{2+} results in increased channel activity for a given ATP concentration, resulting from mixed effects of the MgATP activation and magnesium-independent ATP inhibition, and is reflected in a right-shift in the MgATP dose-response curve, relative to Mg^{2+}-free ATP. The sensitivity of D207E-containing channels to both MgATP and Mg^{2+}-free ATP was reduced ~3-fold in each case, with IC_{50} in Mg^{2+}-free ATP of ~40 and ~55 μM, respectively (Fig. 4).

The relationship between the IC_{50} in ATP in the presence and absence of Mg^{2+} (IC_{50}[MgATP]/IC_{50}[ATP]) can provide an indirect measure of the extent of Mg^{2+}-nucleotide activation. For D207E and WT SUR2A, the IC_{50}[MgATP]/IC_{50}[ATP] was very similar (~1.5), indicating that sensitivity to Mg^{2+} acti-

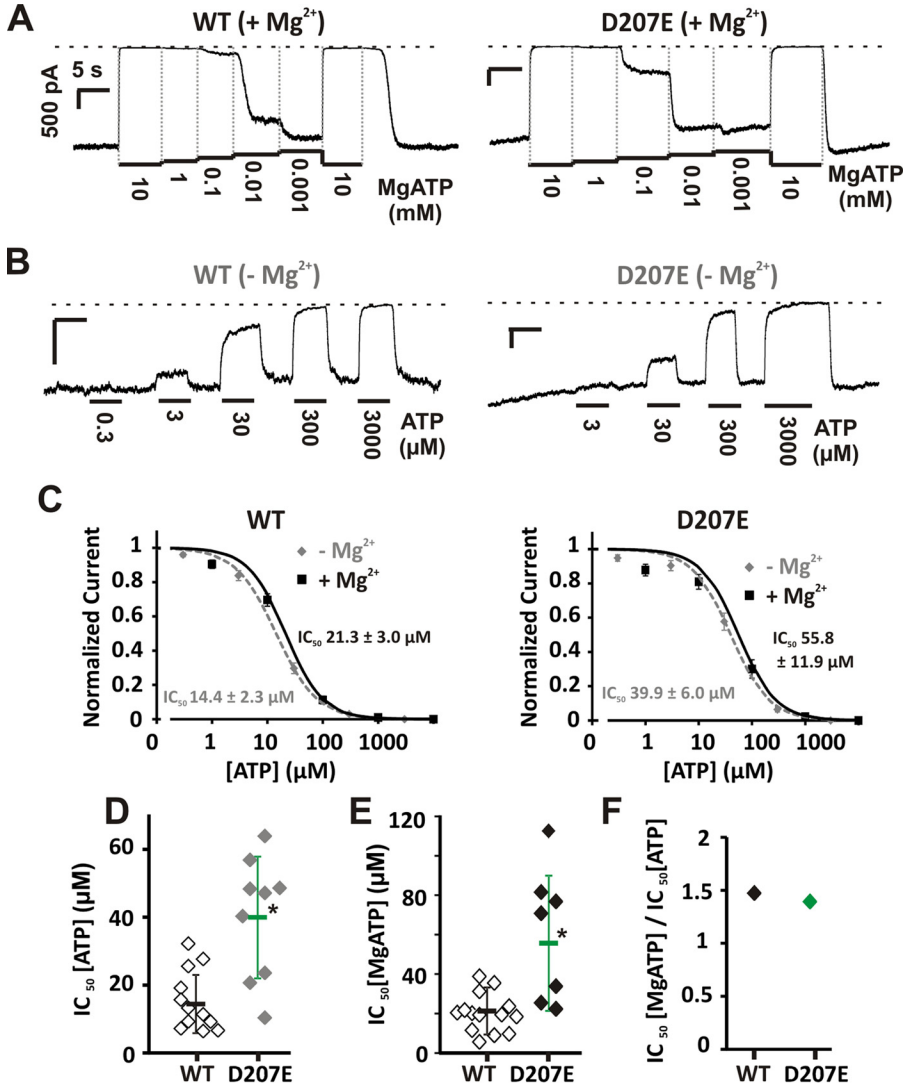

Figure 4. D207E provokes decreases in ATP inhibition in the presence and absence of Mg^{2+}. Inside-out patch-clamp recordings were made from Cosm6 cells transfected with Kir6.2 plus either SUR2A-WT or D207E. The response to MgATP was determined from voltage-clamped patches (−50 mV), as shown in representative traces (*scale bars* denote 500 pA/5 s unless otherwise stated) (*A*). ATP inhibition in the absence of Mg^{2+} was also determined from voltage-clamped patches (−50 mV), as shown in representative traces (*B*). Kir6.2/SUR2A-WT channels were inhibited by ATP in the presence of Mg^{2+} with an IC_{50} of 21.3 ± 3.0 μM (Hill coefficient 1.3 ± 0.1; $n = 16$) and by ATP in the absence of Mg^{2+} with an IC_{50} of 14.4 ± 2.3 μM (Hill coefficient 1.2 ± 0.1; $n = 14$). This was increased in both cases by the D207E mutation; here, the IC_{50} for ATP in the presence of Mg^{2+} was 55.8 ± 11.9 μM (Hill coefficient 1.2 ± 0.1; $n = 9$), and by ATP in the absence of Mg^{2+} with an IC_{50} of 39.9 ± 6.0 μM (Hill coefficient 1.2 ± 0.1; $n = 9$) (*C*). Scatter plots show data from individual experiments with mean IC_{50} ± S.D. *D* and *E,* notably, the ratio of the IC_{50} for ATP in the absence and presence of Mg^{2+} was unchanged by the D207E mutation, indicating the mutation had little effect on Mg^{2+}-nucleotide activation (*F*). Statistical significance is denoted by *asterisk* and defined as $p < 0.05$ according to Mann-Whitney *U* test.

vation was unaffected by this mutation (Fig. 4*F*) and suggesting that GoF results from decreased sensitivity to inhibitory ATP itself. Considering the location of this residue, predicted to be in close proximity to the ATP-binding site on Kir6.1 in the octameric K_{ATP} complex (3, 4), this could conceivably arise from altered binding affinity. Alternatively, decreased ATP sensitivity could be the result of enhanced open-state stability of channels (19, 31). To test the latter directly, we measured the response of channels to PIP_2 perfused onto the intracellular surface of excised membrane patches (Fig. 5). PIP_2 increases open probability (P_o) to ~1, and the ratio of initial current levels to the activated level in PIP_2 provides an estimate of the initial "intrinsic" P_o (28). As shown in Fig. 5, the intrinsic P_o was increased from ~0.4 in WT to ~0.7 in D207E channels. Therefore, the D207E mutation within the L0-linker results in K_{ATP} gain-of-function by increasing the intrinsic open probability of channels, rather than by decreasing inhibitory ATP binding affinity.

Mutations within the Y981/G985/M1056 cluster increase Mg^{2+}-nucleotide activation

The disease-associated mutations Y981S, G985E, and M1056I are all clustered together on transmembrane helices 12 and 13 in TMD2 (Fig. 1). In comparison with WT SUR2A, the IC_{50} for ATP inhibition in the presence of Mg^{2+} was significantly increased by each of these mutations; however, in contrast to D207E, there was no effect on ATP sensitivity in the absence of Mg^{2+} (Fig. 6). This is further demonstrated by the increase in IC_{50}[MgATP]/IC_{50}[ATP] for all mutants (Fig. 6*G*), indicating that the mutations in this cluster of residues linking

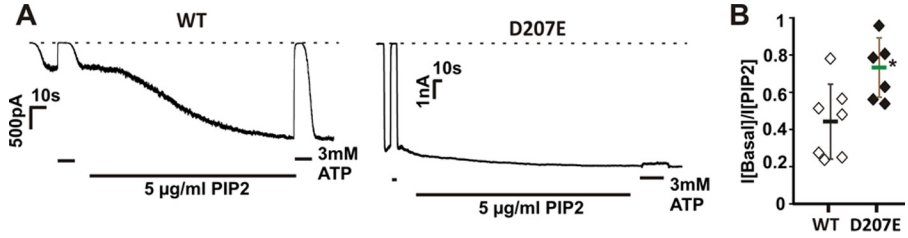

Figure 5. D207E increases intrinsic open-state stability. Inside-out patch-clamp recordings were made from Cosm6 cells transfected with Kir6.2 alongside either SUR2A-WT or D207E. Patches were administered 3 mM ATP followed by washout and administration of 5 μg/ml PIP_2 to maximally increase channel activity, as indicated on representative traces (*A*). The stable peak current observed in PIP_2 was divided by the current observed in the absence of nucleotides/PIP_2 to determine the level of basal channel activity. D207E channels displayed increased basal activity (I[basal]/[PIP_2] was 0.44 ± 0.08 for SUR2A-WT and 0.73 ± 0.06 for D207E; scatter plot shows data from individual experiments with mean ± S.D. from seven patches) (*B*). Statistical significance is denoted by *asterisk* and defined as $p < 0.05$ according to Mann Whitney *U* test.

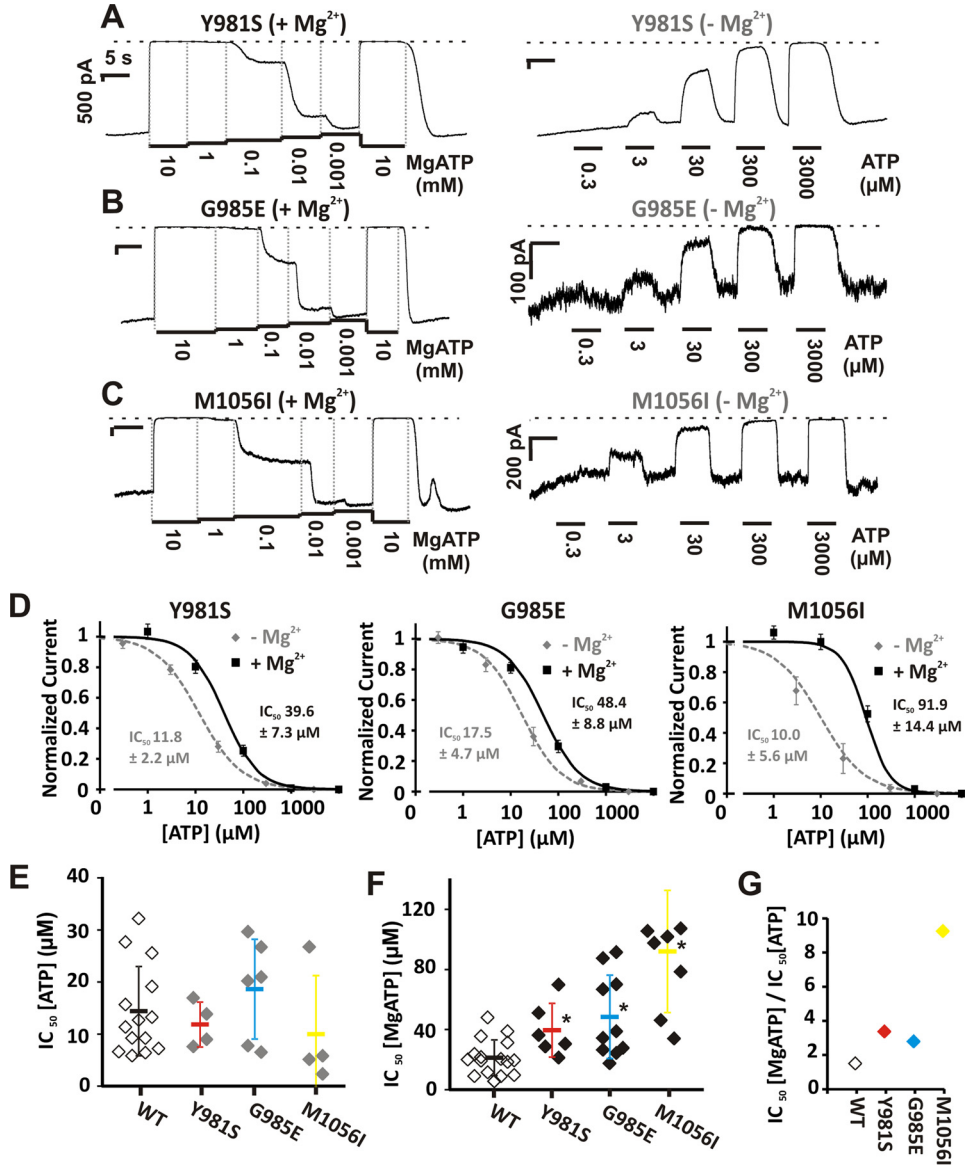

Figure 6. Y981S, G985E, and M1056I cause K_{ATP} GoF by enhancing Mg^{2+}-nucleotide activation. Inside-out patch-clamp recordings were made from Cosm6 cells transfected with Kir6.2 alongside mutant SUR2A. The response to ATP in the presence (*left*) and absence (*right*) of Mg^{2+} was determined from voltage-clamped patches (−50 mV) of cells expressing either Y981S (*A*), G985E (*B*), or M1056I (*C*), as shown in representative traces (*scale bars* denote 500 pA/5 s unless otherwise stated). Analysis of dose-response experiments showed that each mutation increased the IC_{50} for MgATP compared with WT (MgATP IC_{50} for Y981S was 39.6 ± 7.3 μM, Hill coefficient 1.2 ± 0.1, $n = 6$; MgATP IC_{50} for G985E was 48.4 ± 8.7 μM, Hill coefficient 1.1 ± 0.1, $n = 11$; MgATP IC_{50} for M1056I was 91.9 ± 14.4 μM, Hill coefficient 1.7 ± 0.2, $n = 6$), with little effect on ATP inhibition in the absence of Mg^{2+} (ATP IC_{50} for Y981S was 11.8 ± 2.2 μM, Hill coefficient 1.0 ± 0.1, $n = 4$; ATP IC_{50} for G985E was 17.5 ± 4.7 μM, Hill coefficient 1.1 ± 0.1, $n = 6$; ATP IC_{50} for M1056I was 10.0 ± 5.6 μM, Hill coefficient 0.9 ± 0.1, $n = 3$) (*D*). Scatter plots show data from individual experiments with mean IC_{50} ± S.D. (*E* and *F*). Decreased ATP inhibition in the presence of Mg^{2+} only is demonstrated by the ratio of the IC_{50} for ATP in the presence and absence of Mg^{2+}, which is markedly increased for Y981S, G985E, and M1056I (*G*). Statistical significance is denoted by *asterisk* and defined as $p < 0.05$ according to Mann Whitney *U* test.

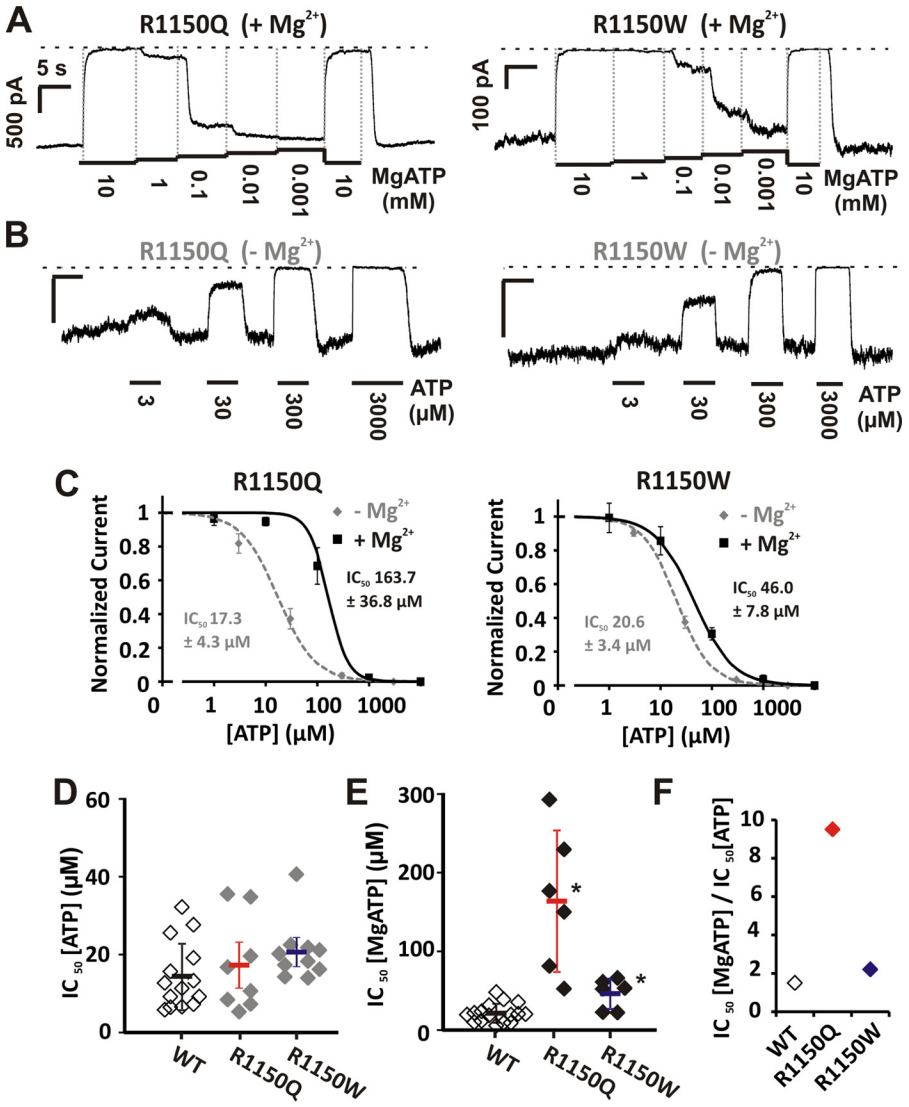

Figure 7. R1150Q and R1150W also cause K_{ATP} GoF by enhancing Mg^{2+}-nucleotide activation. The response to MgATP (*A*) and ATP in the absence of Mg^{2+} (*B*) was determined for channels expressing Kir6.2 with R1150Q or R1150W, by inside-out patch-clamp recordings from Cosm6 cells as shown in representative traces (*scale bars* denote 500 pA/5 s unless otherwise stated). Dose-response analysis (*C*) demonstrated that both mutations markedly increased the IC_{50} for ATP in the presence of Mg^{2+}, compared with WT (MgATP IC_{50} for R1150Q was 163.7 ± 36.8 μM, Hill coefficient 2.3 ± 0.3, $n = 6$; MgATP IC_{50} for R1150W was 46.0 ± 7.8 μM, Hill coefficient 1.2 ± 0.2, $n = 6$). The effect on ATP sensitivity in the absence of Mg^{2+} was more modest for both mutations (ATP IC_{50} for R1150Q was 17.3 ± 4.3 μM, Hill coefficient 1.2 ± 0.2, $n = 8$; ATP IC_{50} for R1150W was 20.6 ± 3.4 μM, Hill coefficient 1.3 ± 0.2, $n = 10$). Scatter plots show data from individual experiments with mean IC_{50} ± S.D. (*D* and *E*). An increase in the ratio of the IC_{50} for ATP in the presence over the IC_{50} for ATP in the absence of Mg^{2+} indicates that these mutations also predominantly confer GoF by augmentation of Mg^{2+}-nucleotide activation (*F*). Statistical significance is denoted by *asterisk* and defined as $p < 0.05$ according to Mann-Whitney *U* test.

NBD1 to TMD2 increase channel activity by enhancing Mg^{2+}-nucleotide activation.

R1150Q and R1150W in TMD2 also enhance Mg^{2+}-nucleotide activation

Having established that the TMD2 Y981S, G985E, and M1056I mutations enhance Mg^{2+}-nucleotide activation, we sought to test whether this mechanism was conserved for other TMD2 mutations, and the most common CS–associated mutations are R1150Q and R1150W. In agreement with a previous report (16), we show that R1150Q causes a large increase in MgATP IC_{50}, whereas R1150W has a more modest effect (Fig. 7). In contrast, R1150Q and R1150W caused only slight increases in ATP IC_{50} (Fig. 7), again reflected in increased IC_{50}[MgATP]/IC_{50}[ATP] for R1150Q and R1150W (Fig. 7*F*), and thus both R1150Q and R1150W cause gain-of-function predominantly by enhancing Mg^{2+}-nucleotide sensitivity.

Effect of CS GoF mutations on glibenclamide sensitivity

Glibenclamide (glyburide) inhibits K_{ATP} channels in a biphasic manner, with high-affinity inhibition arising from interaction with the SUR subunit occurring at nanomolar to micromolar concentrations and low-affinity inhibition due to interaction with the Kir6.x subunit (32). To specifically measure high-affinity inhibition, we applied glibenclamide up to 10 μM. Glibenclamide inhibited WT SUR2A K_{ATP} currents (in the absence of nucleotides), as well as D207E, Y981S, G985E, and M1056I (Fig. 8), with maximal inhibition of ~70% and IC_{50} values ranging from ~15 to 45 nM. In contrast, mutations at residue 1150, in particular R1150W,

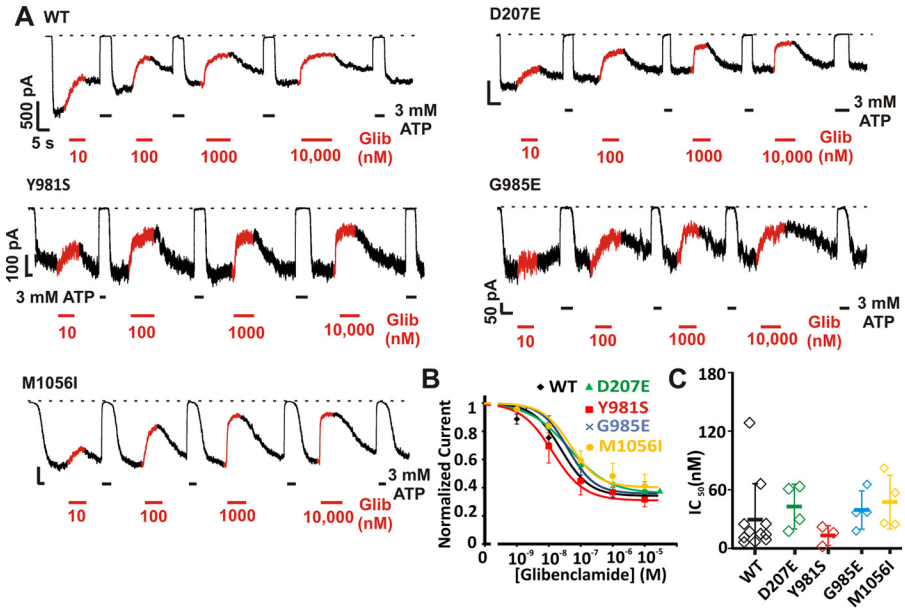

Figure 8. D207E, Y981S, G985E, and M1506I have no significant effect on glibenclamide sensitivity. Inside-out patch-clamp recordings were made from Cosm6 cells transfected with Kir6.2 alongside WT or mutant SUR2A. Reversible inhibition was observed following administration of increasing glibenclamide concentrations, as shown in representative traces (*scale bars* denote 500 pA/5 s unless otherwise stated) (*A*). Dose-response analysis demonstrated that only minor, non-statistically significant variations in glibenclamide IC_{50} values were observed for these mutations (IC_{50} for SUR2A-WT was 29.5 ± 11.1 nM, Hill coefficient 1.0 ± 0.1, $n = 11$; IC_{50} for D207E was 42.8 ± 11.4 nM, Hill coefficient 0.7 ± 0.1, $n = 4$; IC_{50} for Y981S 13.1 ± 5.9 nM, Hill coefficient 0.9 ± 0.1, $n = 3$; IC_{50} for G985E 39.2 ± 9.8 nM, Hill coefficient 1.0 ± 0.2, $n = 4$; IC_{50} for M1056I 47.3 ± 13.8 nM, Hill coefficient 1.0 ± 0.4, $n = 4$) (*B*). Scatter plots show data from individual experiments with mean IC_{50} ± S.D. (*C*). Statistical significance was determined using Mann-Whitney U tests.

resulted in a significant decrease in glibenclamide potency (Fig. 9).

Discussion

Cantu syndrome–associated ABCC9 mutations all cause K_{ATP} GoF

To date, the few analyzed Cantu syndrome–associated mutations in *ABCC9* (SUR2), have been shown to result in gain-of-function of K_{ATP} channels in the presence of Mg^{2+}-nucleotides, which can arise either from decreased sensitivity to inhibitory ATP, or augmented activation by Mg^{2+}-nucleotides (16, 19). In this study, we have demonstrated that four previously uncharacterized mutations in SUR2 (D207E (human D207E), Y981S (Y985S), G985E (G989E), and M1056I (M1060I)) lead to increased channel activity in the presence of regulatory nucleotides via diverse molecular mechanisms. As in previous reports, we used Kir6.2/SUR2A channels for analysis due to the difficulty of recording Kir6.1/SUR2 currents, although it is expected that the mechanism of SUR2 mutations will be conserved irrespective of the pore-forming subunit. In addition, although the dependence of channel activity on intracellular nucleotides differs quantitatively between the two major SUR2 splice variants (SUR2A and SUR2B, which differ only in their C-terminal exon) (33, 34), it is anticipated that, qualitatively, the changes observed for mutant SUR2A-containing channels will be common for SUR2B-containing channels. Interestingly, many CS features such as vascular dilatation and lymphedema likely arise from smooth muscle dysfunction, whereas the effects on cardiac electrophysiology and skeletal muscle are less obvious (24). This may suggest that the biophysical effects of mutations are more severe in SUR2B-containing channels than in SUR2A-containing channels. Alternatively, it is possible that the predominantly smooth muscle consequences of CS arise due to the physiological context of K_{ATP} function in smooth muscle rather than unique biophysical effects on SUR2B compared with SUR2A.

Mechanistic basis of GoF varies between mutations

Here, we compared the sensitivity of wildtype and mutant channels to ATP in the absence and presence of Mg^{2+} to separate the Mg^{2+}-independent inhibitory effect of ATP from the activating effect of MgATP. This analysis shows that the D207E mutation reduces ATP inhibition itself, whereas the Y981S/G985E/M1056I mutations all increase activity by enhancing MgATP activation. The D207E mutation is found in the intracellular L0-linker between the two transmembrane domains TMD0 and TMD1 (Fig. 1). A critical role of the L0-linker in determining channel-gating properties has been suggested for both SUR1 and SUR2 (35, 36). Recent high-resolution structures of the related Kir6.2/SUR1 K_{ATP} channel complex confirm earlier predictions that the L0-linker is closely apposed to the intracellular domains of the Kir6 subunit, and likely it provides a structural interaction between the subunits that is involved in the transduction of functional signals. Interestingly, multiple mutations in the L0-linker of SUR1 have been reported in neonatal diabetes patients, including the analogous mutation to D207E (37). Functional characterization of L0-linker mutations in SUR1 show that channel activity is increased due to elevations in the intrinsic channel open probability, arising from decreased occupation of long-lived, ATP-accessible closed states (35). Consistent with this finding, we show that enhanced basal open probability of D207E-containing channels, reflected in decreased PIP_2 activation, underlies decreased sensitivity to inhibitory ATP (Figs. 4 and 5).

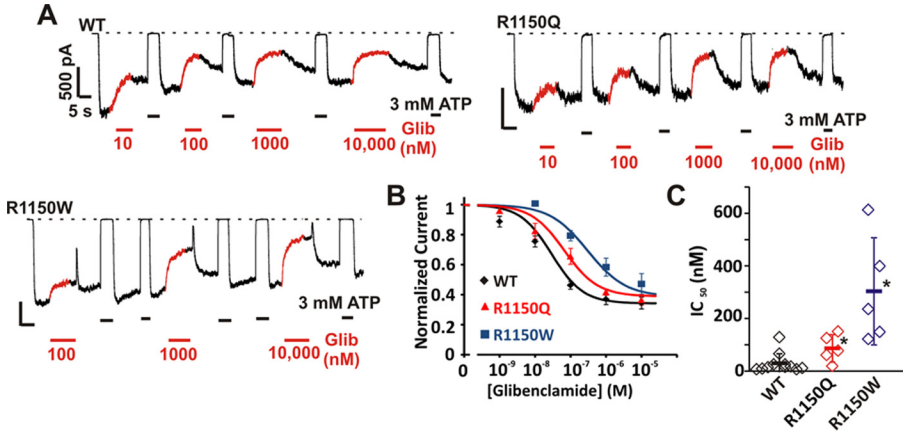

Figure 9. R1150Q and R1150W decrease glibenclamide sensitivity. Glibenclamide sensitivity was measured from inside-out patch-clamp recordings from Cosm6 cells expressing Kir6.2 with either SUR2A-WT, R1150Q, or R1150W as shown in representative traces (*scale bars* denote 500 pA/5 s unless otherwise stated) (*A*). Dose-response analysis shows that both R1150Q and R1150W induce a statistically significant decrease in glibenclamide sensitivity (IC_{50} for R1150Q was 86.3 ± 23.4 nM, Hill coefficient 0.8 ± 0.3, $n = 5$; IC_{50} for R1150W was 303.5 ± 91.1 nM, Hill coefficient 0.8 ± 0.1, $n = 5$) (*B*). Scatter plots show data from individual experiments with mean IC_{50} ± S.D. (*C*). Statistical significance was determined using Mann-Whitney U tests; *, $p < 0.05$.

In contrast, we show that the Y981S, G985E, and M1056I mutations all act by increasing K_{ATP} channel activation by MgATP (Fig. 6). These residues are all predicted to lie in close proximity to each other in a cluster within TMD2; Tyr-981 and Gly-985 are found at the N-terminal end of TM12, immediately following the NBD1-TMD2 linker, whereas M1056I is situated on the opposing TM13 (Fig. 1). The location of the Tyr-981/Gly-985/Met-1056 cluster, at the link between the NBDs and the TM domains (Fig. 1), is appropriate for transduction of movements between the intracellular and transmembrane domains of SUR2. Biochemical analyses of SUR and related ABC proteins indicate that MgADP or MgATP binding to the NBDs of SUR may act to stabilize dimerization of NBD1 and NBD2 (7, 38, 39). However, how binding or NBD dimerization is coupled to gating of the channel pore remains poorly understood.

The concentration of free Mg^{2+} varies in different cell types (40); in cardiomyocytes (which express Kir6.2/SUR2A), free Mg^{2+} is reported to be ~0.5 mM, the concentration used in this study (41). As free Mg^{2+} levels are tightly regulated in most cells, the physiological effect of CS mutations that alter Mg^{2+} nucleotide sensitivity will be altered responses to nucleotide concentrations (in the presence of Mg^{2+}), not to changing Mg^{2+} concentrations (9).

In addition, we show that the previously reported common CS mutations R1150Q and R1150W (located in TM15 of TMD2) also enhance MgATP activation (Fig. 7), demonstrating that multiple transmembrane regions of TMD2 are involved in the conformational changes associated with Mg^{2+}-nucleotide activation.

Notably, the gain-of-function induced by each mutation is quite subtle when mutant and WT SUR2A subunits are co-expressed to mimic the clinically relevant heterozygosity (Fig. 2). Recent reports of GoF mutations in Kir6.2 and SUR1 that underlie neonatal diabetes demonstrate that even very subtle biophysical effects can result in disease (42), suggesting that dramatic changes may not be necessary. In contrast, because SUR2B may be the more pathologically relevant splice variant, it is possible that these mutations will have a greater effect on channels containing SUR2B. In addition, the channel activity measured in $^{86}Rb^{+}$ experiments under basal conditions may not fully recapitulate the metabolic and physiological context for K_{ATP} channels in muscle or other differentiated cell types, and so we cannot rule out a more significant activating effect under other conditions.

Consequences for sulfonylurea sensitivity

Previous studies have demonstrated that second generation sulfonylureas such as glibenclamide inhibit SUR2-containing KATP channels, albeit with lower potency than SUR1-containing channels (43). As such, glibenclamide, or other sulfonylureas, represents a potential pharmacotherapy for CS. However, there are multiple reports of neonatal diabetes mutations in the Kir6.2/SUR1 K_{ATP} subunits that reduce sulfonylurea sensitivity (28, 29) and, as we have recently demonstrated, the CS–associated mutation V65M in Kir6.1 profoundly reduces glibenclamide inhibition of recombinant channels (30). Therefore, it is important to assess the effect of SUR2 CS mutations on inhibitor sensitivity. Here, we show that the D207E, Y981S, G985E, and M1056I mutations do not obviously affect glibenclamide sensitivity (Fig. 8). It has been reported that sulfonylurea inhibition of SUR2-containing channels is affected by nucleotide regulation (44, 45), and so it is possible that these mutations may alter SU sensitivity under more complex physiological regulation, but this remains to be established.

A decrease in glibenclamide potency was observed in both the R1150Q and R1150W mutations (Fig. 9). Interestingly, Arg-1150 lies in TM15 (Fig. 1), and previous studies have demonstrated that TMs 14–16 are critical for high-affinity SU binding to SUR subunits (46, 47). Indeed, serine to tyrosine substitution of a single residue in TM16 (predicted to lie within ~15 Å of Arg-1150 on the cytoplasmic extensions of the TM helix) is sufficient to confer SUR2-like sensitivity to SUR1, and vice versa (46, 47). This raises the possibility that the Arg-1150 mutations may directly decrease glibenclamide sensitivity via disruption of the drug-binding site. The R1150W mutation exhibited a more pronounced effect than the glutamine mutation at the same site, perhaps due to a greater steric effect of the

bulky tryptophan side chain. Regarding the relevance to treatability of disease, it is important to note that glibenclamide sensitivity was evaluated in a "homozygous" context where all SUR2 subunits were mutated, but all CS patients identified so far are heterozygous. The data highlight the relatively minor effect of most mutations on drug sensitivity, although they suggest that the Arg-1150 mutation may reduce SU sensitivity in patients. Potentially, studies of native channels in human-induced pluripotent stem cell-derived cardiovascular cells may allow more accurate assessment of the potential impact of CS mutations on the pharmacological response.

Taken together, these results provide further evidence for K_{ATP} gain-of-function consequences of SUR2 mutations in Cantu syndrome. For several mutations clustered in TM12–13, the results illustrate a common mechanism (enhanced MgATP activation) without marked effect on sulfonylurea sensitivity. The results provide novel insights into the function of K_{ATP} channel complexes, can be useful for linking CS genotype to phenotype in this complex disorder, and will inform the consideration of therapeutic approaches to CS.

Experimental procedures

Molecular biology and cell culture

Mutations were introduced into a rat SUR2A (pCMV_rSUR2A; GenBank™ accession no. D83598.1) cDNA construct using site-directed mutagenesis and verified by direct Sanger sequencing. The residue numbering refers to the rSUR2A clone, which shares 97% sequence identity with the human sequence and was used to allow for comparison with previous reports of the effects of other Cantu syndrome mutations that also used rSUR2A. Cosm6 cells were cultured in Dulbecco's modified Eagle's medium (DMEM) and transfected using FuGENE 6 (Roche Applied Science) with wildtype pcDNA3.1_mKir6.2 (0.6 μg; GenBank™ accession no. D50581.1) and wildtype or mutant pCMV_rSUR2A constructs (1 μg) in addition to 0.2 μg of pcDNA3.1_eGFP for visual detection of successful transfection. To model heterozygous expression of mutant subunits, cells were transfected with WT Kir6.2 along with a 1:1 ratio of WT and mutant rSUR2A (0.5:0.5 μg). Radioactive rubidium efflux experiments were performed 36 h post-transfection, while the excised patch-clamp recordings were made 48–72 h post-transfection.

$^{86}Rb^+$ efflux assay

Transfected Cosm6 cells were plated in 12-well plates to reach 70–80% confluence on the day of experimenting. Prior to commencing the efflux assay, the culture medium was replaced by DMEM supplemented with 1 μCi/ml ^{86}RbCl (PerkinElmer Life Sciences) and incubated for >6 h (37 °C/5% CO_2) to load the cells with the $^{86}Rb^+$ isotope. After the loading incubation, cells were washed with Ringer's solution containing (in mM) 118 NaCl, 10 HEPES, 25 $NaHCO_3$, 4.7 KCl, 1.2 KH_2PO_4, 2.5 $CaCl_2$, and 1.2 $MgSO_4$ either alone or supplemented with 2.5 mg/ml oligomycin and 1 mM 2-deoxy-D-glucose to induce metabolic inhibition (MI) and incubated at room temperature for a further 10 min. Cells were then washed three times with Ringer's solution (either with or without MI supplements) before the experiment was commenced. Ringer's solution was added to each well, collected, and replaced at the defined time points (2.5, 5, 12.5, 22.5, and 37.5 min). After the experiment, cells were lysed with 2% SDS to attain the remaining intracellular $^{86}Rb^+$, and sample radioactivity was determined by scintillation counting.

The cumulative $^{86}Rb^+$ efflux at each time point was calculated from the total counts from each sample (including the $^{86}Rb^+$ remaining post-cell lysis). Apparent K_{ATP}-independent efflux rate constants (k_1) were obtained from GFP-transfected cells using Equation 1,

$$\text{efflux} = 1 - e^{-k_1 \cdot t} \quad \text{(Eq. 1)}$$

and K_{ATP}-dependent efflux rate constant (k_2) was obtained from K_{ATP}-transfected cells using Equation 2,

$$\text{efflux} = 1 - e^{((-k_1 \cdot t) + (-k_2 \cdot t))} \quad \text{(Eq. 2)}$$

where k_1 was obtained from GFP-transfected cells (Equation 1). The number of active channels was assumed to be proportional to k_2. In MI conditions a time-dependent divergence from a mono-exponential efflux is observed. This is attributed to inactivation of background efflux mechanisms over time; therefore, in this condition rate constants were derived from exponential functions fit to early time points only (2.5–12.5 min). Efflux-time data shown represents the mean ± S.E. from at least three independent experiments each with multiple replicates ($N \geq 3$, $n \geq 4$). K_{ATP}-dependent flux rate data is shown as mean ± S.D. Statistical significance was determined using Mann-Whitney *U* tests with a p value <0.05 deemed statistically significant.

Inside-out excised patch-clamp recordings

Pipettes were made from soda lime glass microhematocrit tubes (Kimble) and had a resistance of 1–2 megohms when filled with pipette solution. The bath and pipette solutions (K_{INT}) contained (in mM): 140 KCl, 10 HEPES, 1 EGTA (pH 7.4 with KOH). Currents were recorded at a constant holding potential of −50 mV in the absence and presence of nucleotides as indicated. Where included, free Mg^{2+} concentrations were maintained at 0.5 mM by supplementation of $MgCl_2$ as calculated using CaBuf (Katholieke Universiteit Leuven). Where stated, porcine brain PIP_2 (Avanti Polar Lipids) was applied at 5 μg/ml. Rapid solution exchange was attained using a Dynaflow Resolve perfusion chip (Cellectricon). Experiments were performed at 20–22 °C. K_{ATP} channel currents in solutions of varying nucleotide concentrations were normalized to the basal current in the absence of nucleotides, and dose-response data were fit with a four-parameter Hill fit according to Equation 3, using the Data Solver Function in Microsoft Excel,

$$\text{normalized current} = I_{min} + (I_{max} - I_{min})/(1 + ([X]/IC_{50})^H) \quad \text{(Eq. 3)}$$

where the current in $K_{INT} = I_{max} = 1$; I_{min} is the normalized minimum current observed in ATP/MgATP/glibenclamide; [*X*] refers to the concentration of ATP/MgATP/glibenclamide; IC_{50} is the concentration of half-maximal inhibition; and *H* denotes the Hill coefficient.

Data were tested for statistical significance using the Mann Whitney *U* test, and presented as mean ± S.E. in dose-response plots, and as mean ± S.D. in scatter plots showing IC_{50} values from individual experiments.

Author contributions—C. M., G. v. H., and C. G. N. conceptualization; C. M., A. H., M. S.-R., H. I. R., D. J., D. K. G., and G. v. H. data curation; C. M., A. H., M. S.-R., and C. G. N. formal analysis; C. M. investigation; C. M., G. v. H., and C. G. N. methodology; G. v. H. and C. G. N. funding acquisition.

Acknowledgment—We thank Risha Shah (Washington University) for help with $^{86}Rb^+$ efflux experiments.

References

1. Shyng, S., and Nichols, C. G. (1997) Octameric stoichiometry of the KATP channel complex. *J. Gen. Physiol.* **110,** 655–664 CrossRef Medline
2. Clement, J. P., 4th., Kunjilwar, K., Gonzalez, G., Schwanstecher, M., Panten, U., Aguilar-Bryan, L., and Bryan, J. (1997) Association and stoichiometry of KATP channel subunits. *Neuron* **18,** 827–838 CrossRef Medline
3. Martin, G. M., Yoshioka, C., Rex, E. A., Fay, J. F., Xie, Q., Whorton, M. R., Chen, J. Z., and Shyng, S. L. (2017) Cryo-EM structure of the ATP-sensitive potassium channel illuminates mechanisms of assembly and gating. *Elife* **6,** e24149 Medline
4. Li, N., Wu, J. X., Ding, D., Cheng, J., Gao, N., and Chen, L. (2017) Structure of a pancreatic ATP-sensitive potassium channel. *Cell* **168,** 101–110 CrossRef Medline
5. Nichols, C. G. (2006) KATP channels as molecular sensors of cellular metabolism. *Nature* **440,** 470–476 CrossRef Medline
6. Tucker, S. J., Gribble, F. M., Zhao, C., Trapp, S., and Ashcroft, F. M. (1997) Truncation of Kir6.2 produces ATP-sensitive K^+ channels in the absence of the sulphonylurea receptor. *Nature* **387,** 179–183 CrossRef Medline
7. Nichols, C. G., Shyng, S. L., Nestorowicz, A., Glaser, B., Clement, J. P., 4th, Gonzalez, G., Aguilar-Bryan, L., Permutt, M. A., and Bryan, J. (1996) Adenosine diphosphate as an intracellular regulator of insulin secretion. *Science* **272,** 1785–1787 CrossRef Medline
8. Flagg, T. P., Kurata, H. T., Masia, R., Caputa, G., Magnuson, M. A., Lefer, D. J., Coetzee, W. A., and Nichols, C. G. (2008) Differential structure of atrial and ventricular KATP: atrial KATP channels require SUR1. *Circ. Res.* **103,** 1458–1465 CrossRef Medline
9. Foster, M. N., and Coetzee, W. A. (2016) KATP channels in the cardiovascular system. *Physiol. Rev.* **96,** 177–252 CrossRef Medline
10. Flagg, T. P., Enkvetchakul, D., Koster, J. C., and Nichols, C. G. (2010) Muscle KATP channels: recent insights to energy sensing and myoprotection. *Physiol. Rev.* **90,** 799–829 CrossRef Medline
11. Nelson, M. T., Huang, Y., Brayden, J. E., Hescheler, J., and Standen, N. B. (1990) Arterial dilations in response to calcitonin gene-related peptide involve activation of K^+ channels. *Nature* **344,** 770–773 CrossRef Medline
12. Nakashima, M., and Vanhoutte, P. M. (1995) Isoproterenol causes hyperpolarization through opening of ATP-sensitive potassium channels in vascular smooth muscle of the canine saphenous vein. *J. Pharmacol. Exp. Ther.* **272,** 379–384 Medline
13. Bonev, A. D., and Nelson, M. T. (1993) ATP-sensitive potassium channels in smooth muscle cells from guinea pig urinary bladder. *Am. J. Physiol.* **264,** C1190–C1200 CrossRef Medline
14. Ko, E. A., Han, J., Jung, I. D., and Park, W. S. (2008) Physiological roles of K^+ channels in vascular smooth muscle cells. *J. Smooth Muscle Res.* **44,** 65–81 CrossRef Medline
15. Teramoto, N. (2006) Physiological roles of ATP-sensitive K^+ channels in smooth muscle. *J. Physiol.* **572,** 617–624 CrossRef Medline
16. Harakalova, M., van Harssel, J. J., Terhal, P. A., van Lieshout, S., Duran, K., Renkens, I., Amor, D. J., Wilson, L. C., Kirk, E. P., Turner, C. L., Shears, D., Garcia-Minaur, S., Lees, M. M., Ross, A., Venselaar, H., *et al.* (2012) Dominant missense mutations in ABCC9 cause Cantu syndrome. *Nat. Genet.* **44,** 793–796 CrossRef Medline
17. van Bon, B. W., Gilissen, C., Grange, D. K., Hennekam, R. C., Kayserili, H., Engels, H., Reutter, H., Ostergaard, J. R., Morava, E., Tsiakas, K., Isidor, B., Le Merrer, M., Eser, M., Wieskamp, N., de Vries, P., *et al.* (2012) Cantu syndrome is caused by mutations in ABCC9. *Am. J. Hum. Genet.* **90,** 1094–1101 CrossRef Medline
18. Cooper, P. E., Reutter, H., Woelfle, J., Engels, H., Grange, D. K., van Haaften, G., van Bon, B. W., Hoischen, A., and Nichols, C. G. (2014) Cantu syndrome resulting from activating mutation in the KCNJ8 gene. *Hum. Mutat.* **35,** 809–813 CrossRef Medline
19. Cooper, P. E., Sala-Rabanal, M., Lee, S. J., and Nichols, C. G. (2015) Differential mechanisms of Cantu syndrome-associated gain-of-function mutations in the ABCC9 (SUR2) subunit of the KATP channel. *J. Gen. Physiol.* **146,** 527–540 CrossRef Medline
20. Afifi, H. H., Abdel-Hamid, M. S., Eid, M. M., Mostafa, I. S., and Abdel-Salam, G. M. (2016) *De novo* mutation in ABCC9 causes hypertrichosis acromegaloid facial features disorder. *Pediatr. Dermatol.* **33,** e109–e113 CrossRef Medline
21. Brownstein, C. A., Towne, M. C., Luquette, L. J., Harris, D. J., Marinakis, N. S., Meinecke, P., Kutsche, K., Campeau, P. M., Yu, T. W., Margulies, D. M., Agrawal, P. B., and Beggs, A. H. (2013) Mutation of KCNJ8 in a patient with Cantu syndrome with unique vascular abnormalities–support for the role of K(ATP) channels in this condition. *Eur. J. Med. Genet.* **56,** 678–682 CrossRef Medline
22. Grange, D. K., Lorch, S. M., Cole, P. L., and Singh, G. K. (2006) Cantu syndrome in a woman and her two daughters: further confirmation of autosomal dominant inheritance and review of the cardiac manifestations. *Am. J. Med. Genet. A* **140,** 1673–1680 Medline
23. Leon Guerrero, C. R., Pathak, S., Grange, D. K., Singh, G. K., Nichols, C. G., Lee, J. M., and Vo, K. D. (2016) Neurologic and neuroimaging manifestations of Cantu syndrome: a case series. *Neurology* **87,** 270–276 CrossRef Medline
24. Nichols, C. G., Singh, G. K., and Grange, D. K. (2013) KATP channels and cardiovascular disease: suddenly a syndrome. *Circ. Res.* **112,** 1059–1072 CrossRef Medline
25. Levin, M. D., Zhang, H., Uchida, K., Grange, D. K., Singh, G. K., and Nichols, C. G. (2015) Electrophysiologic consequences of KATP gain-of-function in the heart: Conduction abnormalities in Cantu syndrome. *Heart Rhythm* **12,** 2316–2324 CrossRef Medline
26. Levin, M. D., Singh, G. K., Zhang, H. X., Uchida, K., Kozel, B. A., Stein, P. K., Kovacs, A., Westenbroek, R. E., Catterall, W. A., Grange, D. K., and Nichols, C. G. (2016) K(ATP) channel gain-of-function leads to increased myocardial L-type Ca^{2+} current and contractility in Cantu syndrome. *Proc. Natl. Acad. Sci. U.S.A.* **113,** 6773–6778 CrossRef Medline
27. Li, A., Knutsen, R. H., Zhang, H., Osei-Owusu, P., Moreno-Dominguez, A., Harter, T. M., Uchida, K., Remedi, M. S., Dietrich, H. H., Bernal-Mizrachi, C., Blumer, K. J., Mecham, R. P., Koster, J. C., and Nichols, C. G. (2013) Hypotension due to Kir6.1 gain-of-function in vascular smooth muscle. *J. Am. Heart Assoc.* **2,** e000365 Medline
28. Koster, J. C., Remedi, M. S., Dao, C., and Nichols, C. G. (2005) ATP and sulfonylurea sensitivity of mutant ATP-sensitive K^+ channels in neonatal diabetes: implications for pharmacogenomic therapy. *Diabetes* **54,** 2645–2654 CrossRef Medline
29. Proks, P. (2013) Neonatal diabetes caused by activating mutations in the sulphonylurea receptor. *Diabetes Metab. J.* **37,** 157–164 CrossRef Medline
30. Cooper, P. E., McClenaghan, C., Chen, X., Stary-Weinzinger, A., and Nichols, C. G. (2017) Conserved functional consequences of disease-associated mutations in the slide-helix of Kir6.1 and Kir6.2 subunits of the ATP-sensitive potassium channel. *J. Biol. Chem.* **292,** 17387–17398 CrossRef Medline
31. Proks, P., Antcliff, J. F., Lippiat, J., Gloyn, A. L., Hattersley, A. T., and Ashcroft, F. M. (2004) Molecular basis of Kir6.2 mutations associated with neonatal diabetes or neonatal diabetes plus neurological features. *Proc. Natl. Acad. Sci. U.S.A.* **101,** 17539–17544 CrossRef Medline
32. Gribble, F. M., and Reimann, F. (2003) Sulphonylurea action revisited: the post-cloning era. *Diabetologia* **46,** 875–891 CrossRef Medline

33. Matsuoka, T., Matsushita, K., Katayama, Y., Fujita, A., Inageda, K., Tanemoto, M., Inanobe, A., Yamashita, S., Matsuzawa, Y., and Kurachi, Y. (2000) C-terminal tails of sulfonylurea receptors control ADP-induced activation and diazoxide modulation of ATP-sensitive K^+ channels. *Circ. Res.* **87,** 873–880 CrossRef Medline
34. Reimann, F., Gribble, F. M., and Ashcroft, F. M. (2000) Differential response of KATP channels containing SUR2A or SUR2B subunits to nucleotides and pinacidil. *Mol. Pharmacol.* **58,** 1318–1325 Medline
35. Babenko, A. P., and Bryan, J. (2003) Sur domains that associate with and gate KATP pores define a novel gatekeeper. *J. Biol. Chem.* **278,** 41577–41580 CrossRef Medline
36. Fang, K., Csanády, L., and Chan, K. W. (2006) The N-terminal transmembrane domain (TMD0) and a cytosolic linker (L0) of sulphonylurea receptor define the unique intrinsic gating of KATP channels. *J. Physiol.* **576,** 379–389 CrossRef Medline
37. Ellard, S., Flanagan, S. E., Girard, C. A., Patch, A. M., Harries, L. W., Parrish, A., Edghill, E. L., Mackay, D. J., Proks, P., Shimomura, K., Haberland, H., Carson, D. J., Shield, J. P., Hattersley, A. T., and Ashcroft, F. M. (2007) Permanent neonatal diabetes caused by dominant, recessive, or compound heterozygous SUR1 mutations with opposite functional effects. *Am. J. Hum. Genet.* **81,** 375–382 CrossRef Medline
38. Zingman, L. V., Alekseev, A. E., Bienengraeber, M., Hodgson, D., Karger, A. B., Dzeja, P. P., and Terzic, A. (2001) Signaling in channel/enzyme multimers. *Neuron* **31,** 233–245 CrossRef Medline
39. Ueda, K., Komine, J., Matsuo, M., Seino, S., and Amachi, T. (1999) Cooperative binding of ATP and MgADP in the sulfonylurea receptor is modulated by glibenclamide. *Proc. Natl. Acad. Sci. U.S.A.* **96,** 1268–1272 CrossRef Medline
40. Swaminathan, R. (2003) Magnesium metabolism and its disorders. *Clin. Biochem. Rev.* **24,** 47–66 Medline
41. Quamme, G. A., and Rabkin, S. W. (1990) Cytosolic free magnesium in cardiac myocytes: identification of a Mg^{2+} influx pathway. *Biochem. Biophys. Res. Commun.* **167,** 1406–1412 CrossRef Medline
42. Vedovato, N., Cliff, E., Proks, P., Poovazhagi, V., Flanagan, S. E., Ellard, S., Hattersley, A. T., and Ashcroft, F. M. (2016) Neonatal diabetes caused by a homozygous KCNJ11 mutation demonstrates that tiny changes in ATP sensitivity markedly affect diabetes risk. *Diabetologia* **59,** 1430–1436 CrossRef Medline
43. Gribble, F. M., Tucker, S. J., Seino, S., and Ashcroft, F. M. (1998) Tissue specificity of sulfonylureas: studies on cloned cardiac and beta-cell K(ATP) channels. *Diabetes* **47,** 1412–1418 CrossRef Medline
44. Hambrock, A., Löffler-Walz, C., and Quast, U. (2002) Glibenclamide binding to sulphonylurea receptor subtypes: dependence on adenine nucleotides. *Br. J. Pharmacol.* **136,** 995–1004 CrossRef Medline
45. Proks, P., de Wet, H., and Ashcroft, F. M. (2014) Sulfonylureas suppress the stimulatory action of Mg-nucleotides on Kir6.2/SUR1 but not Kir6.2/SUR2A KATP channels: a mechanistic study. *J. Gen. Physiol.* **144,** 469–486 CrossRef Medline
46. Ashfield, R., Gribble, F. M., Ashcroft, S. J., and Ashcroft, F. M. (1999) Identification of the high-affinity tolbutamide site on the SUR1 subunit of the K(ATP) channel. *Diabetes* **48,** 1341–1347 CrossRef Medline
47. Hambrock, A., Löffler-Walz, C., Russ, U., Lange, U., and Quast, U. (2001) Characterization of a mutant sulfonylurea receptor SUR2B with high affinity for sulfonylureas and openers: differences in the coupling to Kir6.x subtypes. *Mol. Pharmacol.* **60,** 190–199 Medline